# Supplementary Materials for

## Obesity Remodels Activity and Transcriptional State of a Lateral Hypothalamic Brake on Feeding

Mark A. Rossi†, Marcus L. Basiri†, Jenna A. McHenry, Oksana Kosyk, James M. Otis, Hanna E. van den Munkhof, Julien Bryois, Christopher Hübel, Gerome Breen, Wilson Guo, Cynthia M. Bulik, Patrick F. Sullivan, and Garret D. Stuber*

† Equal contribution
Correspondence to: gstuber@uw.edu

**This PDF file includes:**

**Materials and Methods**

Subjects and surgery

Adult Vglut2-IRES-Cre (Vglut2-Cre, Jackson Labs stock no. 028863) (*24*) were used for all behavioral and imaging experiments unless otherwise noted. Specific details regarding age and sex are given for each experiment in the corresponding methods section. All procedures were conducted in accordance the NIH guide for the care and use of laboratory animals and were approved by the Institutional Animal Care and Use Committee at the University of North Carolina. For all stereotaxic surgeries, mice were anaesthetized with isoflurane (3% induction, maintained at 1-1.5%) and placed within a stereotaxic frame (Kopf). Ophthalmic ointment was placed on the eyes and topical anesthetic (lidocaine) was applied to the incision site. During surgeries, viruses were administered to the perifornical lateral hypothalamic area at AP (from Bregma) -1.3 mm, ML (from Bregma) +/-0.9-1.0 mm, DV (from brain surface) -5.1 mm. All viruses were infused through custom stainless steel injectors at a rate of 100 nL/min. Injectors were left in place for at least 10 min following each infusion. Following surgery mice were maintained on ad lib. acetaminophen (in drinking water) for 3 days. Mice were monitored daily and allowed to recover for at least one week before any dietary manipulations began and at least 3 weeks before stimulation or imaging began to allow for viral infection. All viruses were packaged at the University of North Carolina Vector Core.

Optogenetics

*ChR2 validation*

Vglut2-Cre mice (n = 4; female; 3-4 months at time of surgery) were injected bilaterally in LHA with AAVdj-DIO-ChR2-eYFP (500 nl per hemisphere). Six weeks after injections, mice were deeply anesthetized with pentobarbital and transcardially perfused with ice-cold sucrose cutting solution containing (in mM): 225 sucrose, 119 NaCl, 1.0 $NaH_2P0_4$, 4.9 $MgCl_2$, 0.1 $CaCl_2$, 26.2 $NaHCO_3$, 1.25 glucose, 303 mOsm. Brains were rapidly removed and coronal sections were taken at 300 um. Sections were incubated in aCSF at 32 degrees C containing (in mM): 119 NaCl, 2.5 KCl, 1.0 $NaH_2P0_4$, 1.3 $MgCl_2$, 2.5 $CaCl_2$, 26.2 $NaHCO_3$, 15 glucose, 310 mOsm. Whole cell recordings were taken using borosilicate pipettes (4-7 MΩ) backfilled with solution containing (in mM):

130 potassium gluconate, 10 KCl, 10 HEPES, 10 EGTA, 2 $MgCl_2$, 2 ATP, 0.2 GTP (pH 7.35, 270–285 mOsm).

To assess spike fidelity, laser pulses were delivered through the objective via a 470 nm LED (ThorLabs) during current clamp recordings. Pulse trains were 3 s in duration with 5 ms square pulses at 1, 5, 10, 20, and 40 Hz. Spike fidelity was calculated from the entire 3 s pulse train. Spike fidelity varied as a function of pulse frequency in fluorescent cells in the LHA (n = 7 cells from 3 mice; one-way ANOVA, $F(4,24) = 16.66$, $p = 1.16x10\text{-}6$). However, the number of spikes elicited per 3 s pulse train increased with pulse frequency ($F(4,24) = 23.66$, $p = 4.96x10\text{-}8$). To assess local connectivity, voltage clamp recordings were performed from non-fluorescent cells located near fluorescent cells within the LHA. Brief light pulses elicited strong inward currents in 62% (8/13 cells in 4 mice) of non-fluorescent cells that were blocked by the AMPA receptor antagonist DNQX (100%, 2/2 cells in 2 mice).

*Surgery and behavior*

Male Vglut2-Cre mice aged 2-6 months were injected bilaterally in LHA with AAV5-DIO-ChR2-eYFP (n = 12) or AAV5-DIO-eYFP (n = 5). Optic fibers (200 μm core diameter) were implanted ~150 μm above the injection site and cemented in place (*25*). A stainless steel head-fixing ring was also cemented atop each mouse's head. Approximately 4 weeks after surgery, behavioral testing started. Mice were habituated to head fixation for two 10-min sessions in which sucrose rewards were randomly delivered. Mice were headfixed and connected to a 473-nm DPSS laser. Test sessions consisted of 40 trials in which 2μL of 10% sucrose solution was randomly delivered via a tube placed directly in front of the mouse's mouth. Laser stimulation (1-40 Hz, 5 ms pulse width for 3 s, 10 mW) was delivered concurrently with sucrose on 50% of trials. The stimulation frequency was constant during a session but pseudo-randomized between sessions. Licks were recorded during the entire session.

Two mice (one eYFP and one ChR2) were excluded from RTPP testing because their headcaps came loose prior to testing. RTPP was conducted in a rectangular two-chamber box in which the mouse's position was tracked from above with Ethovision (Noldus). Mice were habituated to the chamber for one day prior to testing. On test days,

mice were connected to a 473-nm laser and one side of the chamber (randomized between sessions) was designated as the stimulation side. Sessions lasted 20 min. Laser stimulation was delivered when mice were in the designated stimulation side. Stimulation frequency was randomized between mice.

Following completion of behavioral experiments, mice were perfused and brains were post-fixed in PFA for 24 hr. Sections were taken at 40 μm and imaged using a Zeiss 780 confocal microscope to verify virus expression and fiber placement within the LHA.

Two-photon imaging of LHA-Vglut2 activity dynamics

*GCaMP6m validation*

Vglut2-Cre mice (n = 2, both female, 9 weeks old at time of surgery) were injected bilaterally in LHA with AAVdj-DIO-GCaMP6m (500 nL per hemisphere, 1:2 dilution). Six weeks after injections, mice were deeply anesthetized with pentobarbital and transcardially perfused with ice-cold sucrose cutting solution containing (in mM): 225 sucrose, 119 NaCl, 1.0 $NaH_2P0_4$, 4.9 $MgCl_2$, 0.1 $CaCl_2$, 26.2 $NaHCO_3$, 1.25 glucose, 303 mOsm. Brains were rapidly removed and coronal sections were taken at 300 um. Sections were incubated in aCSF at 32 degrees C containing (in mM): 119 NaCl, 2.5 KCl, 1.0 $NaH_2P0_4$, 1.3 $MgCl_2$, 2.5 $CaCl_2$, 26.2 $NaHCO_3$, 15 glucose, 310 mOsm. Whole cell recordings were taken using borosilicate pipettes (4-7 MΩ) backfilled with solution containing (in mM): 130 potassium gluconate, 10 KCl, 10 HEPES, 10 EGTA, 2 $MgCl_2$, 2 ATP, 0.2 GTP (pH 7.35, 270–285 mOsm).

Whole cell current clamp recordings from fluorescently labeled cells were performed while simultaneously imaging GCaMP6m fluorescence using a microscope-mounted camera (OptiMos, QImaging) and imaging software (MicroManager). Cells were induced to spike at 1-20 Hz by injecting 2-ms current pulses. Offline, ROIs were drawn over the cells and time series data were extracted using ImageJ. Data were normalized by background fluorescence and expressed as proportion change from baseline (mean of 10 frames prior to each pulse train). A total of 10 healthy, GCaMP6m-expressing cells were recorded. Two cells were excluded from analysis because they failed to fire single action potentials in response to current pulses.

*Surgery, behavior, and diet manipulation*

AAVdj-DIO-GCaMP6m (*26*) (500 nL 1:2 dilution) was infused into LHA. A GRIN lens (7.3 mm length, 0.6 mm diameter; Inscopix) was slowly lowered into place (*27*) above the injection site and cemented in place in the center of a circular head-fixing ring (n = 13 male mice). Experiments began four weeks after surgery. Mice were habituated to head fixation for at least two 15-min sessions in which sucrose solution was periodically delivered via a spout directly in front of their mouths. Once mice were habituated to the imaging setup, imaging experiments began. Each imaging session consisted of two parts: first basal activity dynamics were imaged during rest for 10 min. Immediately after this baseline scan, sucrose trials began. Mice were presented with 10 randomly-delivered sucrose rewards (~2 uL per trial; ITI 25-50 s) and licks were monitored throughout the session. To assess activity dynamics related to satiety state, mice were either fed (free access to chow in home cage for at least 24 hr prior to testing) or fasted (no access to chow in home cage for 24 hr prior to testing).

Following completion of satiety experiments, the mice were randomly assigned to either control (n = 6) or HFD groups (n = 7). HFD was 60% animal fat calories (Bio-Serv product #F3282) and the control diet was 16% fat calories (Bio-Serv product #F4031). During the 12-week diet manipulation, mice were maintained on ad lib. access to either control or HFD, and food intake and body weight were monitored throughout to confirm the onset of diet-induced obesity. At two week intervals, cells were imaged on two consecutive days in both the fasted and fed conditions (conducted identically to the initial satiety experiments). Two control mice were not imaged during the 12-week time point because no cells were visible. Data from the fasted state only are shown for the obesity experiments.

*Data Acquisition, signal extraction, and analysis*

Calcium dynamics were monitored through the GRIN lens with a two-photon microscope (Olympus) equipped with resonant scanners (allowing up to 30 Hz collection) and GaAsP PMT as described previously (*19*). A long working distance 20x air objective designed for optical transmission of infrared wavelengths (Olympus, LCPLN20XIR, 0.45 NA, 8.3 mm WD) was used with a tunable Mai-Tai Deep See laser

system (Spectra Physics, ~100 fs pulse width) set to 955 nm for 2p excitation. Prior to each imaging session, FOVs were manually aligned with standard deviation projections from the previous imaging session to ensure the same cells were imaged on consecutive days. Images were collected at 5 Hz and processed with FluoView (Olympus) software. Baseline dynamics were monitored for 10 min at 5 Hz collection rate. During sucrose delivery experiments, images were collected for 20 s around sucrose delivery. Rarely, mice did not lick within 10 s of sucrose delivery, and these trials were excluded post hoc. Following data acquisition, videos were motion corrected using a planar hidden Markov model (SIMA v1.3). Regions of interest (ROIs) were hand drawn and manually tracked across imaging sessions. Time series data were extracted per ROI and analyzed using custom Python software. Events were detected and quantified using custom software described previously(*18*). Briefly, motion-corrected time series data from all ROIs recorded during the 10 min baseline session were z-score normalized and smoothed with a rolling average of 3 frames. Events were defined as transients that exceeded 1.5 standard deviations and lasted at least 2 s. The analysis was also performed on non-z-scored data, and results were similar to those presented. Neuropil decontamination was performed on a subset of the data (452 neurons from 13 mice) using Fast Image Signal Separation Analysis (FISSA). Pearson correlations between the raw and decontaminated signals were 0.91 ±0.003 (mean ±s.e.m.), and the difference between the raw and decontaminated fluorescence signals was 3.5 ± 0.71%. Because neuropil contamination was negligible, further analyses were conducted without neuropil decontamination.

To classify cellular responses as either ‘excited’ or ‘inhibited’ during sucrose consumption, the fluorescent signal for each ROI was averaged across the sucrose consumption period (the first 3 s after the first consummatory lick) and compared to the average response from the frames immediately preceding the consummatory frames for all trials using the Wilcoxon signed-rank test ($p < 0.05$). To test whether calcium activity dynamics could be used to decode the mouse’s behavioral state, we used the Python module scikitlearn with GridSearchCV and a support vector classification that was optimized using linear or radial basis function (rbf) kernels with C parameter ranges $10^{-3}$, $10^{-2}$, $10^{-1}$, $10^{0}$, $10^{1}$, $10^{2}$, $10^{3}$ for both and gamma range $10^{-3}$, $10^{-2}$, $10^{-1}$, $10^{0}$, $10^{1}$, $10^{2}$, $10^{3}$ for rbf using the average and maximum fluorescent signal during the 3 s window after the

first consummatory lick. Data from both fasted and fed conditions were pooled. The model was tested using 1000 iterations in which 90% of cells were randomly selected. Quantification of the performance was done using 10-fold validation. For each run, the highest accuracy score across the tested parameters was considered the model's accuracy of predicting satiety state (fasted or fed). To test whether the predictive ability of the model was greater than chance, the same procedure was conducted using the same data with shuffled satiety state assignments. p-values were calculated comparing the distribution of the decoding accuracy from the data set with the decoding accuracy using shuffled data using the Benjamini-Hochberg correction. Following HFD exposure, calcium dynamics in response to sucrose consumption were used to decode group assignment using the same procedure. Baseline calcium dynamics (mean event amplitude, mean event AUC, mean event duration, mean inter-event interval, number of events, and minimum and maximum values) were used to decode group assignment using the procedure described above.

To test whether the fluorescent signal was correlated with licking during sucrose consumption on a single-cell level, we calculated the lick rate during the 1-s interval following the first lick after sucrose delivery and compared this with the average and maximum fluorescent responses of each cell during the same epoch for every trial of the pre-obesity test. To test whether the population activity was correlated with licking we used a similar approach but instead of using the response from each cell, the responses of all cells within an FOV were averaged on a trial-by-trial basis.

Slice electrophysiology from obese mice

Vglut2-Cre mice (n = 8; 3 months at time of surgery) were injected bilaterally in LHA with AAV5-DIO-eYFP (500 nL per hemisphere). One week after injections, mice were randomly assigned to either control or HFD groups and maintained on ad lib. diet for 6 weeks prior to electrophysiological recordings. On the day of recording, mice were deeply anesthetized with pentobarbital and transcardially perfused with ice-cold sucrose cutting solution containing (in mM): 225 sucrose, 119 NaCl, 1.0 $NaH_2P0_4$, 4.9 $MgCl_2$, 0.1 $CaCl_2$, 26.2 $NaHCO_3$, 1.25 glucose, 303 mOsm. Brains were rapidly removed and coronal sections were taken at 300 um. Sections were incubated in aCSF at 32 degrees C

containing (in mM): 119 NaCl, 2.5 KCl, 1.0 $NaH_2P0_4$, 1.3 $MgCl_2$, 2.5 $CaCl_2$, 26.2 $NaHCO_3$, 15 glucose, 310 mOsm. Targeted recordings were made from fluorescently-labeled cells within the LHA. For excitability experiments, whole cell recordings were taken using borosilicate pipettes (4-7 MΩ) backfilled with solution containing (in mM): 130 potassium gluconate, 10 KCl, 10 HEPES, 10 EGTA, 2 $MgCl_2$, 2 ATP, 0.2 GTP (pH 7.35, 280 mOsm). Current was injected for 800 ms in 25 pA steps ranging from -75 pA to 125 pA. For EPSC/IPSC experiments, the internal solution contained (in mM): 117 Cs-methanesulfonate, 20 HEPES, 0.4 EGTA, 2.8 NaCl, 5 TEA, 5 ATP, 0.5 GTP (pH 7.35, 280 mOsm).

A total of 65 cells from 8 mice were recorded for excitability analysis. Four cells were excluded because of unstable access resistance. Ten cells were excluded because access resistance was >30 MOhms. Of 51 cells included, 30 were eYFP+ (15 control/15 HFD) and 21 were eYFP- (13 control/8 HFD). One eYFP+ cell from the HFD group was excluded based on the Grub test for outliers on rheobase. Cell resistance was calculated from the slope of the I-V curve. Decoding of group assignment was performed as described above using rheobase and the maximum latency to spike from eYFP+ and eYFP- cells.

For EPSC/IPSC recordings, 33 eYFP+ cells were recorded from 8 mice. Thirteen were excluded because access resistance was >30MOhms or because the recording was unstable for both EPSC and IPSC recording. A total of 20 eYFP+ neurons were included in analyses (10 control/10 HFD). Cells were clamped at -70 mV for EPSC recordings and +10 for IPSC recordings. Events were detected using Clampfit.

In situ quantification

Male wild-type mice (n = 4/group, littermates of the mice used for DropSeq experiments) were maintained on ad lib. access to either HFD or control diet for two months. They were then anesthetized and rapidly decapitated. Brains were quickly removed and fresh frozen at -80°C. Sections were cut at 18 μm, mounted on slides, and stored at -80°C under RNase-free conditions. Sections were fixed in 4% PFA for 15min at 4°C, dehydrated in serial ethanol concentrations (50-100%) and processed with RNAscope (Advanced Cell Diagnostics, cat. No. 320293). Sections were hybridized with

the following mixed probes: Vglut2 (Mm-Vglut2 (Slc17a6) cat. no. 319171) and Vgat (Mm-Vgat (Slc31a1) cat. no. 319191) and either Enpp2 (Mm-Enpp2 cat. no. 402441), Nts (Mm-Nts cat. no. 420441), Sst (Mm-Sst cat. no. 404631), or Adcyap1 (Mm-Adcyap1 cat. no. 405911) for 2 h at 40°C. Following amplification, sections were counterstained with DAPI.

Images were acquired with a Zeiss LSM 780 confocal microscope and Zen software using a 20x air objective. Images were acquired using the same microscope settings for each quantified image. For co-localization, circular ROIs were drawn around all DAPI-expressing cells in the LHA using ImageJ. These ROIs were used to determine whether intensity for each fluorophore crossed a threshold that was unique to each fluorophore. Background intensity values were obtained from ROIs drawn within the LHA in places that lacked cell bodies and subtracted per channel from the intensities of cellular ROIs. Each hemisphere was treated independently.

DropSeq

*Tissue Isolation and Preparation of Single-Cell Suspensions*

Male wild-type mice (1 month old at the start of diet manipulation) were maintained on either control (n = 7) or HFD (n = 7) diet for 9-16 weeks. The age of diet manipulation onset differs from the imaging experiments in which mice were >3 months old. Mice were deeply anesthetized with 390 g/kg sodium pentobarbital, 500 mg/kg phenytoin sodium and rapidly transcardially perfused with 20 mL ice-cold sodium-substituted aCSF (NMDG-aCSF: 96 mM NMDG, 2.5 mM KCl, 1.35 mM $NaH_2PO_4$, 30 mM $NaHCO_3$, 20 mM HEPES, 25 mM glucose, 2 mM thiourea, 5 mM $Na^+$ascorbate, 3 mM $Na^+$pyruvate, 0.6 mM glutathione-ethyl-ester, 2 mM N-acetyl-cysteine, 0.5 mM $CaCl_2$, 10 mM $MgSO_4$; pH 7.35–7.40, 300-305 mOsm*)* modified from(*28*). Brains were isolated and six 280 μm sections through the LHA were collected in ice-cold NMDG-aCSF on a vibratome**.** Sections were allowed to recover in carbogen-buffered NMDG-aCSF containing 500 nM TTX, 10 μM APV, 10 μM DNQX (NMDG-aCSF-R) at room temperature for 40 minutes. After recovery, LHA tissue was isolated with Palkovitz punches and incubated in NMDG-aCSF-R containing 1.0 mg/mL pronase for 35 minutes at 30ºC. Following digestion, tissue was transferred to 1.0 mL NMDG-aCSF-R

supplemented with 0.05% BSA (NMDG-aCSF-BSA) and mechanically dissociated with a patch pipet fire-polished to an internal diameter of 200-300 μm. The suspension was washed in 12 mL NMDG-aCSF-BSA, sedimented at 220 x *g* for 6 minutes at 18ºC, and immediately resuspended at a final concentration of 400 cells/μL in NMDG-aCSF-BSA for single-cell capture.

*Drop-seq and single-cell cDNA library preparation*

Drop-seq was performed as described in (*12*) with minor modifications. Single-cell capture was performed on a glass microfluidics device (Dolomite Microfluidics) with flow rates set to manufacturer recommendations. Beads were loaded at a concentration of 390 beads/μL. Reverse transcription, exonuclease I digestion, and PCR were performed as in (*12*) with one additional cycle added to the second stage of amplification. Following PCR, products were pooled by animal, purified on SPRI beads (Agilent) at ratios described in (*12*), and indexed following Nextera XT Tagmentation instructions with 750 *p*g input per reaction. Tagmentation products were double purified on SPRI beads using a negative/positive selection strategy to retain species between 300-600 bp, as quantified with an Agilent Bioanalyzer 2100 High Sensitivity DNA assay. Final libraries were pooled by mass proportional to the estimated number of cells per pool member as quantified by a Qubit dsDNA HS Assay. Sequencing was performed at the UNC High Throughput Sequencing Facility on an lllumina HiSeq2500 using Paired-End 2x50 Rapid Run v2 chemistry.

*Single-Cell Sequencing Clustering and Analysis*

Demultiplexing was performed with 1 mismatch allowed using Illumina bcl2fastq v2.18.0.12. Initial processing and generation of digital expression matrices was performed using Drop-seq_tools v1.12 and Picard Tools v2.2.4 as described in (*12*). Alignment was performed using STAR v2.4.2a with 72 GB of RAM and 16 threads.

Clustering was performed using a combination of Seurat v1.4.0.16 and custom code in R v3.3.2 unless otherwise noted. For clustering of all cells (**Fig. 1**), cells were filtered by ≤ 5,000 and ≥ 200 unique genes, ≤ 15,000 unique molecules, and ≤ 10 percent mitochondrial reads; Filtered data were scaled to the median number of unique molecules and log(x+1) transformed. Zero-variance genes were removed from the data, and batch correction was performed with ComBat (*29*) from the SVA v3.220 (*30*) package using parametric adjustments on a model matrix containing sequencing pool, total number of unique genes and molecules, and percent mitochondrial reads. Batches for clustering were defined as described (**Fig. S1E**). Relative log expression by cell and mean expression correlation across animals were used to assess correction quality (**Fig. S1D**). Only genes detected in all animals by group were included in downstream analysis.

Highly variable genes were selected as described in (*31*) using an implementation in the package M3Drop v1.0.0 (*32*) with a false discovery rate of 0.01 and a minimum dispersion of 0.5. These genes were used as the basis for principal components analysis. Cluster calling was performed on principal components using the Louvain algorithm with multilevel refinement and default settings. Principal components were reduced and visualized via t-distributed stochastic neighbor embedding (tSNE) using the first 100 components and a resolution of 0.5 (**Fig. 1**) under default settings. Clusters were reordered based on a dendrogram estimated on a hierarchically-clustered distance matrix constructed on all genes.

Feature discovery was performed using a likelihood-ratio test for single cell data (*33*) as implemented in Seurat. For cluster features, all genes in each cluster were tested against those in either the nearest cluster or node in the dendrogram tree. For group features, intra-cluster group comparisons were performed using the same test **(Supplementary Data S1)**. In the clustering of all cells, one neuronal cluster comprising 3.72% of all neurons lacked high confidence markers and was not further analyzed (gray in **Fig. 1C**). Comparisons of gene expression levels between groups were performed on inverse hyperbolic sine (asinh) transformed data **(Supplementary Data S1)** (*34*).
For gene *x*,

asinh fold-change (asinhFC) was defined as:

$$asinhFC = ln\left(\left\langle x_{HF}\right\rangle + \sqrt{\left\langle x_{HF}\right\rangle^2 + 1}\right) - ln\left(\left\langle x_C\right\rangle + \sqrt{\left\langle x_C\right\rangle^2 + 1}\right)$$

Signal-to-noise ratio (SNR, **Fig. 2A**) was defined as:

$$SNR = \frac{\left\langle asinh\left(x_C\right)\right\rangle}{\sigma_{asinh\left(X_{HF}\right) - median\left(asinh\left(X_C\right)\right)}}$$

with *HF* denoting high fat group expression and *C* defining control group expression.

All steps from prepossessing to the generation of digital expression matrices were run on a Dell blade-based cluster running RedHat Enterprise Linux 5.6. Cluster calling and tSNE were run on a similar cluster running RedHat Enterprise Linux 7.3. All other steps were run on macOS 10.13.3.

Pseudotime and Functional Annotation Analyses

Pseudotime analysis is an unsupervised algorithm that organizes cells according to their degrees and patterns of transcriptional change to construct trajectories. Cells grouped along branches of these trajectories exhibit similar patterns of transcriptional alteration, and the degree of change between individual cells in a trajectory is referred to as pseudotime. This analysis can therefore be used to describe non-uniform changes across a complex population of cells. Pseudotime analysis was performed using Monocle v2.2.0 (*16*). Briefly, cells from the glutamate cluster were selected and filtered for cells containing ≤ 5,000 and ≥ 500 unique genes, ≤ 15,000 unique molecules, and ≤ 5 percent mitochondrial reads. Raw counts were fit to a negative binomial distribution in which fixed variance and size factors for individual cells were estimated using a mean-geometric-mean-total calculation. DEGs between control and HFD were estimated on a dispersion model and those with q ≤ 0.01 and detected in at least 10% of cells were used for pseudotime ordering. Trajectories were constructed using discriminative dimensionality reduction via learning a tree on two components. A likelihood-ratio test for single cell data was used to identify genes differentially expressed between the top

and bottom quintile of HFD cells ordered by pseudotime (see *Single-Cell Sequencing Clustering and Analysis* Methods and **Supplementary Data S2***)*.

Differentially expressed genes with (likelihood-ratio test, $p \leq 0.001$; **Supplementary Data S1**) were selected as input for functional annotation analysis using ENRICHr (http://amp.pharm.mssm.edu/Enrichr/) (*17*). Adjusted *p*-values from ENRICHr were used to identify significant terms from the following annotation databases: α, GO_Biological_Process_2018, σ, GO_Cellular_Component_2018, υ, GO_Molecular_Function_2018, ξ, KEGG_2016, ρ, Panther_2016, μ, Reactome_2016 (**Supplementary Data S2**).

Single Cell GWAS Association

We used MAGMA (*35*) (v1.06), as described previously (*36*), to identify cell types associated with body mass index (BMI). The GWAS on BMI was a cross-sectional analysis of 353,972 European participants from the UK Biobank. Body composition was assessed using Tanita BC-418 MA scale (Tanita Corporation, Arlington Height, IL). We included 7,794,483 genotyped and imputed SNPs and insertion-deletion variants with a MAF of 1% (referred to as SNPs). We excluded pregnant participants or females afterhysterectomy and covaried for factors related to assessment center, genotyping batch, smoking status, alcohol consumption, menopause, and for continuous measures of age, and socioeconomic status (measured by the Townsend Deprivation Index). We accounted for underlying population stratification by including the first six ancestry PCs, calculated on the European subsample. We used BGENIE v1.2 (https://jmarchini.org/bgenie) for sex-specific analyses and meta-analyzed these sex-specific GWASs using METAL (*37*) (http://csg.sph.umich.edu/abecasis/metal).

Linkage disequilibrium (LD) score regression (*38*) estimated SNP-$h^2$ for BMI was 21.9% (SE = 0.7%), the intercept 1.09 (SE = 0.01), and the attenuation ratio 0.06 (SE = 0.01), indicating a polygenic trait. Significantly associated SNPs ($p < 5 \times 10^{-8}$) were considered as potential index SNPs. SNPs in LD ($r^2 > 0.2$) with a more strongly associated SNP within 3000 kb were assigned to the same locus using Functional Mapping and Annotation (FUMA)(*39*). Overlapping clumps additionally were merged

with a second clumping procedure in FUMA merging all lead SNPs with $r^2$ = 1 to 238 independent genome-wide significant genomic loci.

Genotyping, imputation, and quality control were performed as follows: Blood samples were genotyped on two arrays, which share nearly all of their content: the UKBileve array ($N$ = 49,949) or the UK Biobank Axiom array ($N$ = 438,414). Genotyping was conducted by Affymetrix and was distributed across 33 different batches of approximately 4,700 samples. UK Biobank provides extensive information on sample processing on its web site, biobank.ctsu.ox.ac.uk/crystal/refer.cgi?id=155583. UK Biobank performed stringent quality control on the genotyping data at the Wellcome Trust Centre for Human Genetics (WTCHG). For further details, see: biobank.ctsu.ox.ac.uk/crystal/refer.cgi?id=155580. Prior to imputation, all variant sites with a call rate below 90% were filtered out. Imputation was carried out by UK Biobank using a merged UK10K-1000 Genomes Phase 3 reference panel and the Haplotype Reference Consortium (HRC) panel (*40*) (for further information, see (*41*)). UK Biobank preferentially retained SNPs imputed to HRC for SNPs present in both imputation panels. Imputation was conducted using the IMPUTE4 program.

Furthermore, we excluded non-European participants identified by k-means clustering ($k$ = 4) on the first two principal components derived from the genotype data, and we excluded related individuals (KING relatedness metric >0.088, equivalent to a relatedness value of 0.25). SNPs were excluded if they had a minor allele frequency (MAF) smaller than 1%, if no call was made in more than 2% of samples following imputation, if they were imputed with low confidence (INFO <0.8), if they deviated substantially from Hardy-Weinberg equilibrium (HWE test, $p < 10^{-7}$), or if they were not genotyped and not part of the HRC reference panel (*40*).

A measure of specificity was computed for each gene in each cell type by dividing the expression of a gene in a given cell type by the total expression of the gene in all cell types (range of specificity: 0-1). For each cell type, we then binned the specificity measure into 41 bins (0 representing a gene not expressed in the tissue/cell type, 1 genes in the bottom 2.5% quantile of specificity, …, 40 genes that are in the 97.5% to 100% most specific genes in the tissue/cell type). We then used MAGMA to test for a positive correlation between binned tissue specificity and gene-level genetic

association with BMI for each cell type. The gene-level genetic association was computed with MAGMA (v1.06) using a window surrounding the gene by 35kb upstream to 10kb downstream of the gene. The gene-level association is computed by summing the association p-value of SNPs located in the gene windows taking into account the LD structure of the region. MAGMA also takes into account confounders such as gene length and gene-gene correlation.

Statistics

Optogenetics and imaging data were analyzed using GraphPad Prism and custom Python code that leveraged the Scipy Statistics package. All statistical tests were two-sided and corrected for multiple comparisons where appropriate. DropSeq data were processed and analyzed using a combination of custom *R* code and publicly available packages (detailed above). Code is available at https://github.com/stuberlab. Detailed statistical analyses can be found in **Table S1.**

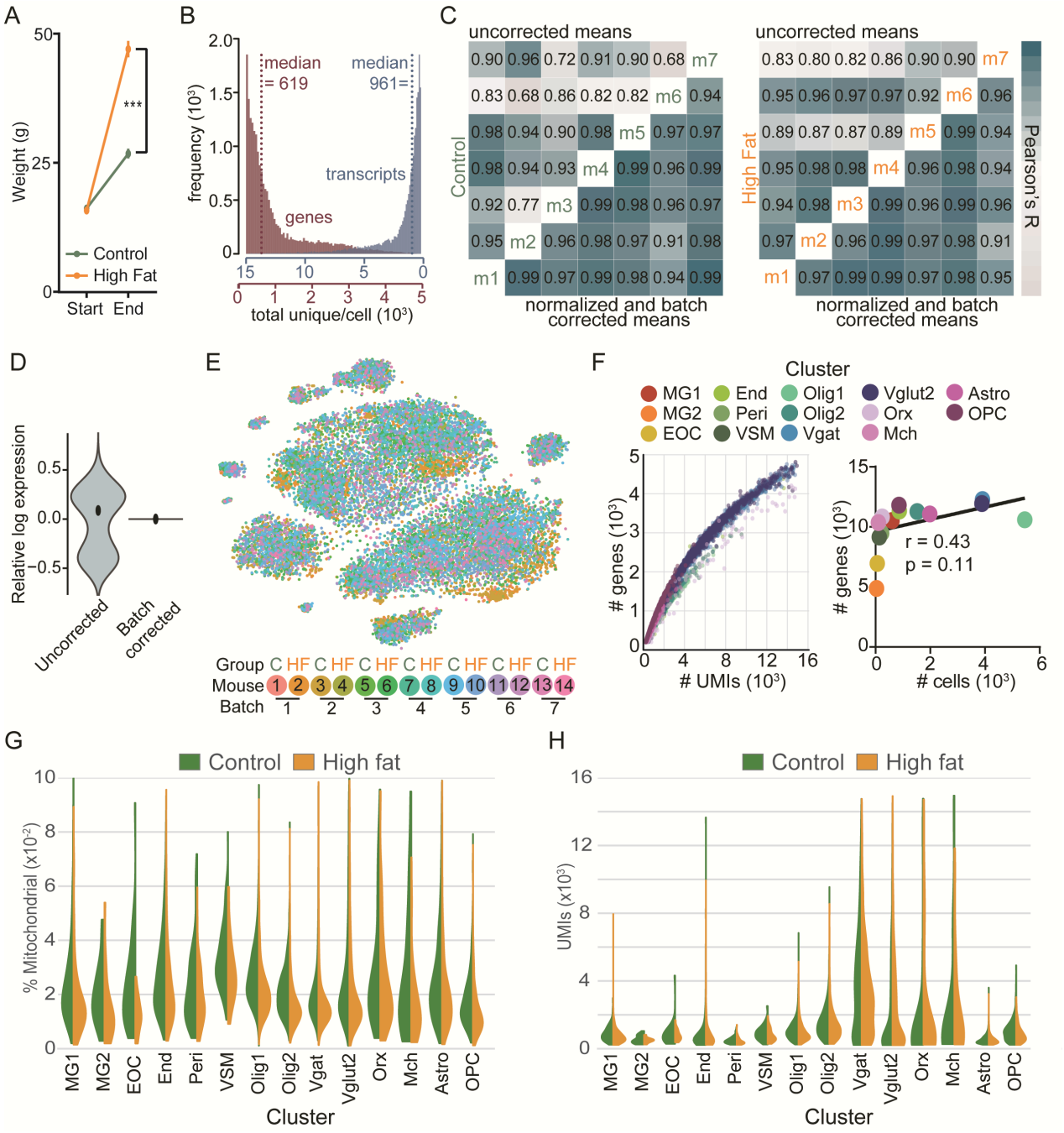


**Fig. S1. DropSeq quality control. A.** Body weight increased following chronic HFD (***p<0.001). Error bars are s.e.m. **B.** Distribution of genes and transcripts per cell. C**.** Correlation matrices for before and after batch correction. m1-m7 correspond to individual mice. **D.** Relative log expression before and after batch correction. **E.** tSNE plot following batch correction. Each color corresponds to a unique mouse. **F.** The number of unique genes detected varied as a function of number of unique molecular

identifiers (UMIs) similarly across all clusters (left). The number of genes detected per cluster was independent of cluster size (right). **G.** Percent mitochondrial genes detected across all clusters. **H.** Number of UMIs detected across all clusters.

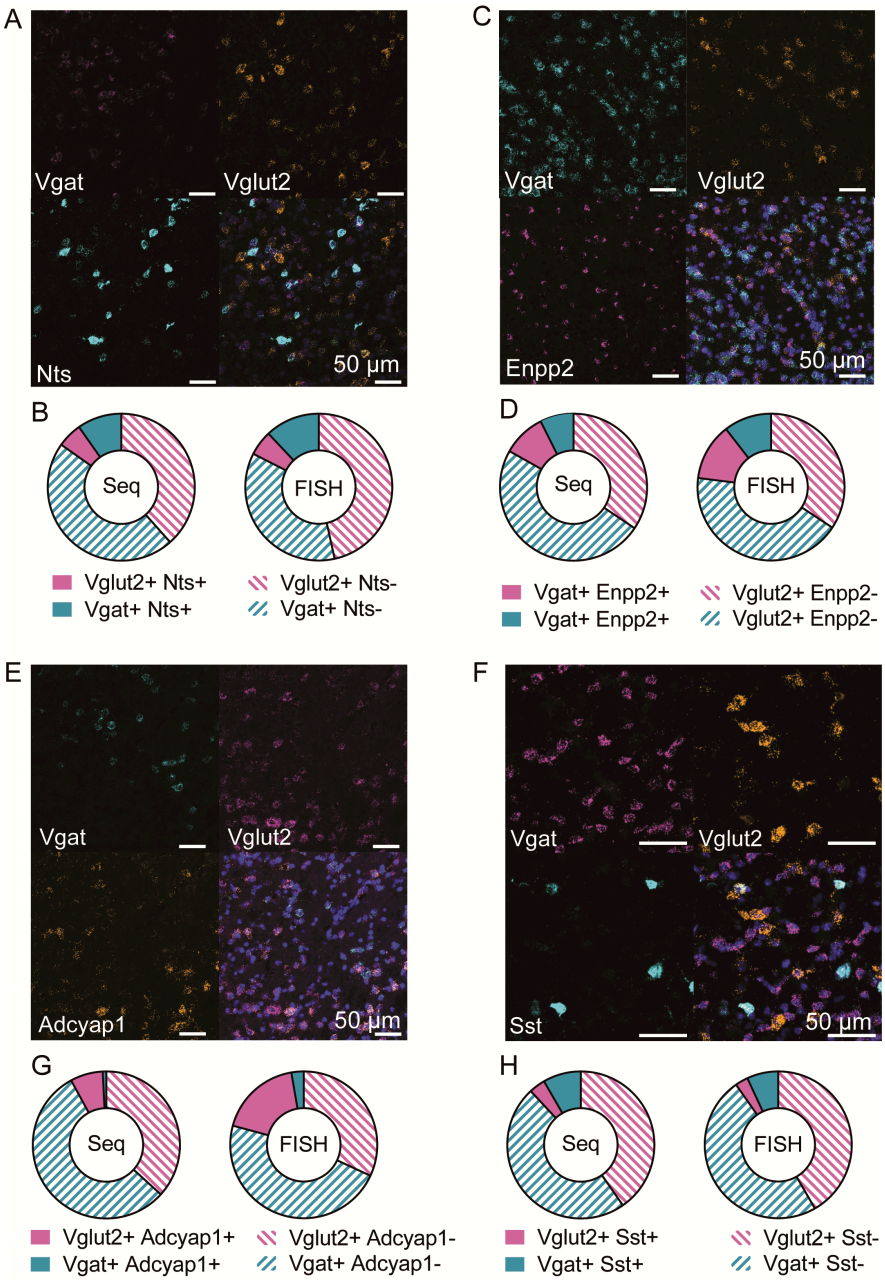


**Fig. S2.** ***In situ*** **validation of sequencing. A.** Fluorescent *In situ* hybridization (FISH) of Vgat (*Slc32a1*), Vglut2 (*Slc17a6*), and Neurotensin (*Nts)*. **B.** Proportions of single- and double-labeled cells are similar between single-cell sequencing and FISH. Single-cell sequencing and FISH single- and double-labeling were qualitatively similar between modalities for *Enpp2* (**C-D**), *Adcyap1* (**E-F**), and *Sst* (**G-H**). For each experiment, data are quantified from the LHA of 6 mice (3 high fat and 3 control; 2 hemispheres per mouse, >9,000 cells per FISH experiment).

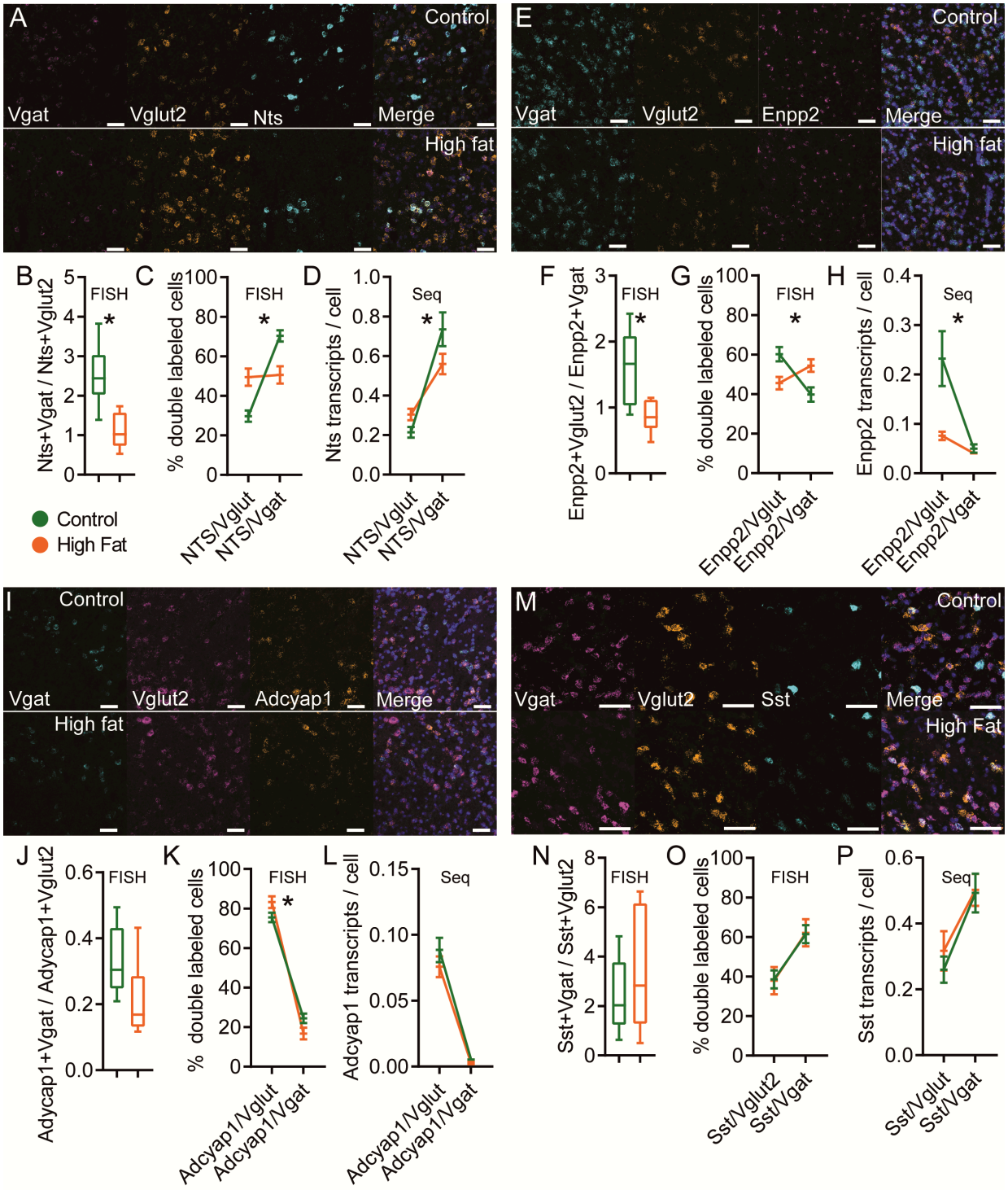


**Fig. S3.** ***In situ*** **validation of diet effects.** Unique patterns of transcriptional changes resulting from HFD were validated for four genes by fluorescence *in situ* hybridization (FISH). **A.** FISH of Vgat, Vglut2, and Nts. Blue is dapi stain on merged images. **B.** The ratio of Nts/Vgat to Nts/Vglut2 co-localizing cells using FISH was reduced by HFD ($p$ =

0.004). Boxes indicate quartiles; lines indicate range. **C.** The percentage of double-labeled cells that express either Nts/Vglut2 or Nts/Vgat using FISH was altered by obesity ($X^2 = 95.84$, $p < 0.0001$). **D.** The expression level within Nts/Vglut2 and Nts/Vgat cells detected by sequencing was modified by HFD differentially in the Vglut2 and Vgat clusters ($p = 0.0105$). Sequencing and FISH data were comparable for *Enpp2* (**E-H**), *Adcyap1* (**J-L**), and *Sst* (**M-P**). For each experiment, data are quantified from the LHA of 6 mice (3 high fat and 3 control; 2 hemispheres per mouse, >9,000 cells per FISH experiment). Scale bars are 50 μm. Error bars in **C**, **D**, **G**, **H**, **K**, **L**, **O**, and **P** are s.e.m. * $p < 0.05$.

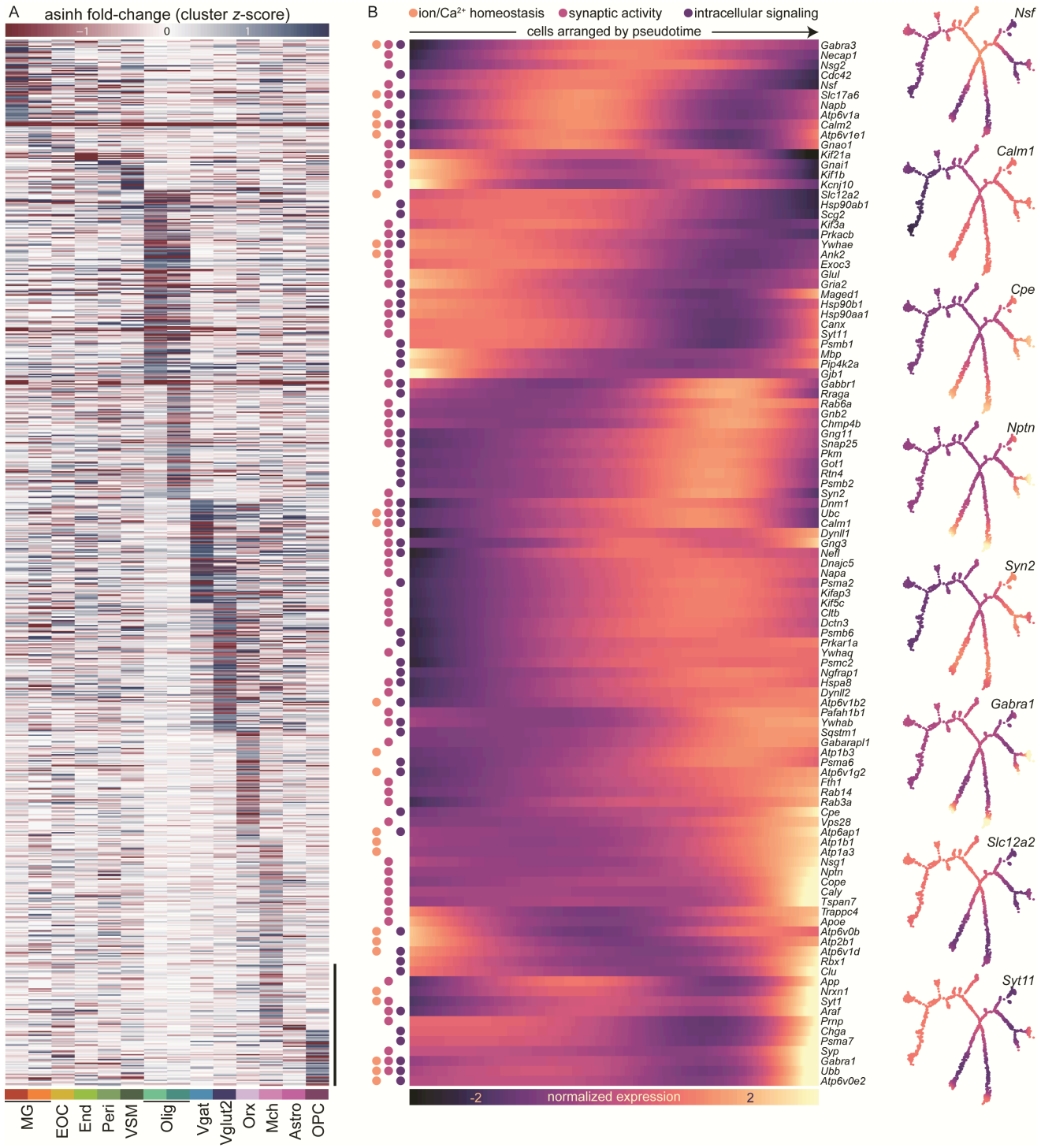


**Fig. S4. Differential gene expression across clusters and genes comprising annotation classes altered in LHA$^{Vglut2}$ neurons demonstrate pseudotime-dependent expression patterns. A.** Differential gene expression between HFD and control cells across clusters. Differential gene expression was assessed between HFD and control cells

within each cluster individually. Positive values indicate upregulation in HFD mice relative to controls. Scale bar, 100 genes. Data are subset from **Supplementary Data S1** (genes expressed in ≥10% of cells, asinFC ≥0.05, $p$ ≥0.0001. 858 genes total). **B.** Expression of genes associated with functional annotation classes enriched in $LHA^{Vglut2}$ HFD cells show distinct expression patterns across the pseudotime space. Cells (columns) are arranged by pseudotime. Dots (left) represent gene-wise membership in select annotation classes suggestive of changes in neuronal activity dynamics (**Fig. 2H**). Expression of example genes across the $LHA^{Vglut2}$ trajectory is shown to the right.

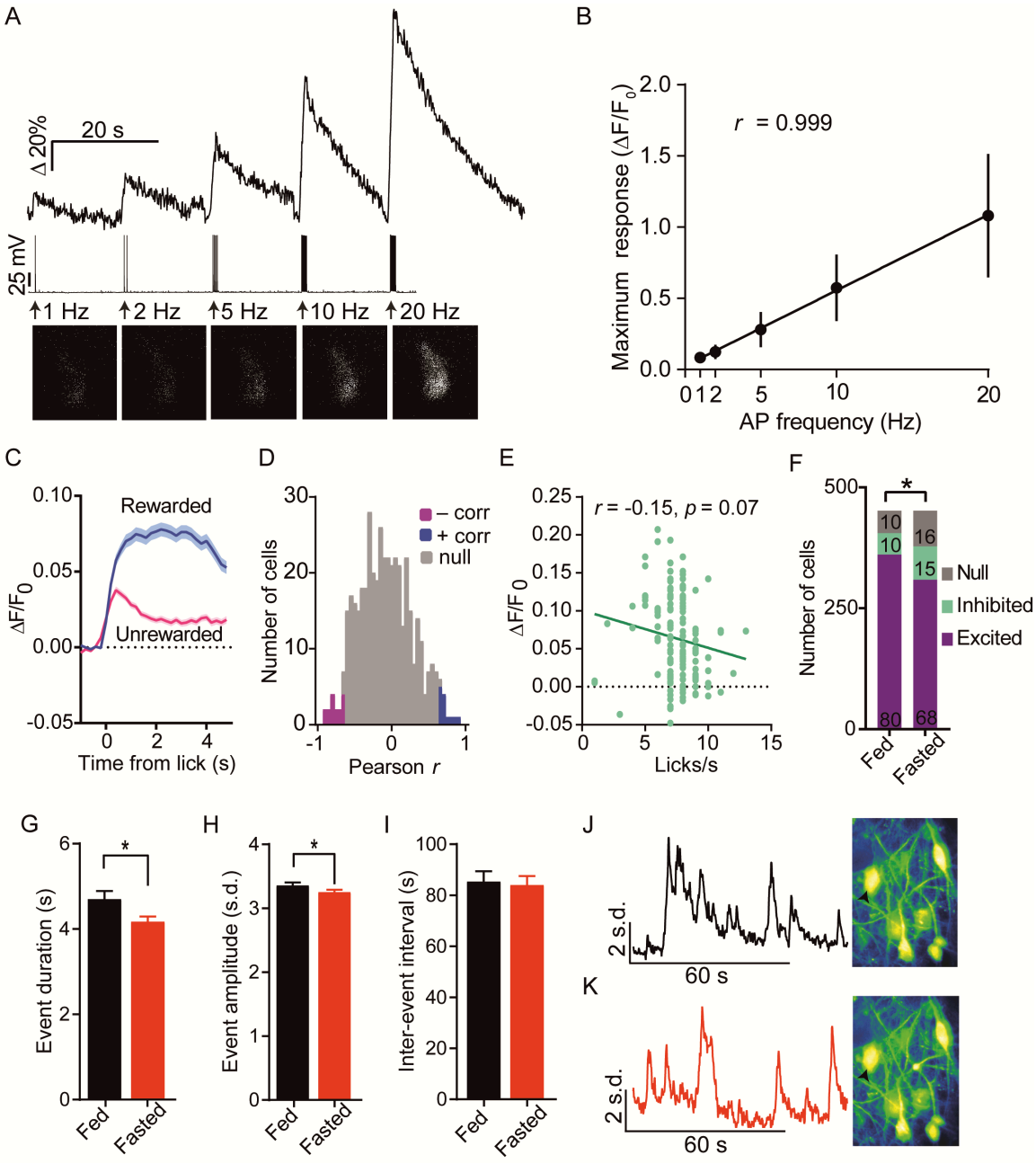


**Fig. S5. GCaMP6m validation, satiety baseline, and relationship between licking and fluorescence. A.** Example of LHA$^{Vglut2}$ cell expressing GCaMP6m. Cells were held at -70 mV and 1-ms current pulses were injected to elicit 1-20 spikes while fluorescence was monitored. Extracted fluorescent signal for the cell is on top, simultaneously-recorded voltage is in the middle, and the frame corresponding to the peak fluorescent signal is on the bottom. Representative images are filtered (yen filter 130-199) and made black and white for display purposes only. **B.** Maximum fluorescence intensity plotted as

a function of action potential frequency. n = 8 cells from 2 mice. **C.** Population fluorescence response to rewarded and unrewarded licks. **D.** Distribution of individual neuron correlations with lick rate. Colored bars represent neurons whose activity is significantly correlated with licking ($p<0.05$; 15/452 negatively correlated, 13/452 positively correlated). **E.** Population activity (average fluorescence for all ROIs in each field of view) was not correlated with the lick rate on a trial-by-trial basis. **F.** The number of neurons that were significantly excited, inhibited, or unresponsive (null) to sucrose consumption is altered by satiety. Fewer neurons are excited when mice are fasted compared with when they are fed ($X^2(2) = 15.59$, $p = 0.0004$). Numbers inside the bars indicate percent of cells. **G.** Event duration was reduced by fasting ($p = 0.0037$). **H.** Event amplitude was reduced by fasting ($p = 0.013$). Only neurons with events in both conditions were included (n = 331). **I.** Inter-event interval was unaffected by fasting ($p = 0.77$). Only neurons with 2 or more events were included (n = 262). **J.** Example fluorescent trace from an $LHA^{Vglut2}$ neuron (arrow) recorded from a fed mouse. **K.** Fluorescent trace from the same neuron as **J** recorded when the mouse is fasted. Error bars are s.e.m.

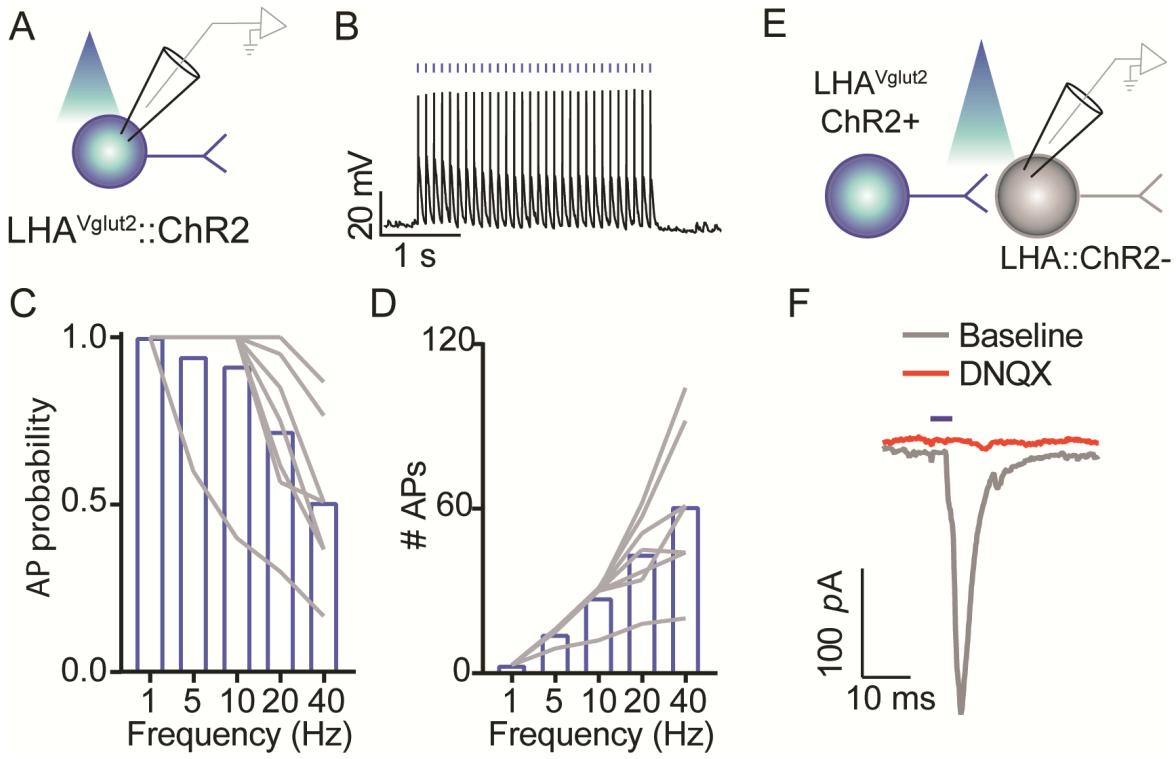


**Fig. S6. ChR2 validation.** **A**. Schematic of experiment. **B.** Whole-cell patch clamp electrophysiology of an LHA$^{Vglut2}$ neuron showing reliable spiking in response to blue light. **C.** Probability of light-evoked spiking varies as a function of stimulation frequency. **D.** The total number of action potentials elicited by 3 s pulse trains varies as a function of stimulation frequency. **E**. Schematic of experimental design. **F**. Whole-cell patch clamp recording from eYFP-negative LHA cell. Blue light elicits an inward current that is blocked by the glutamate receptor antagonist, DNQX (2/2 cells from 2 mice).

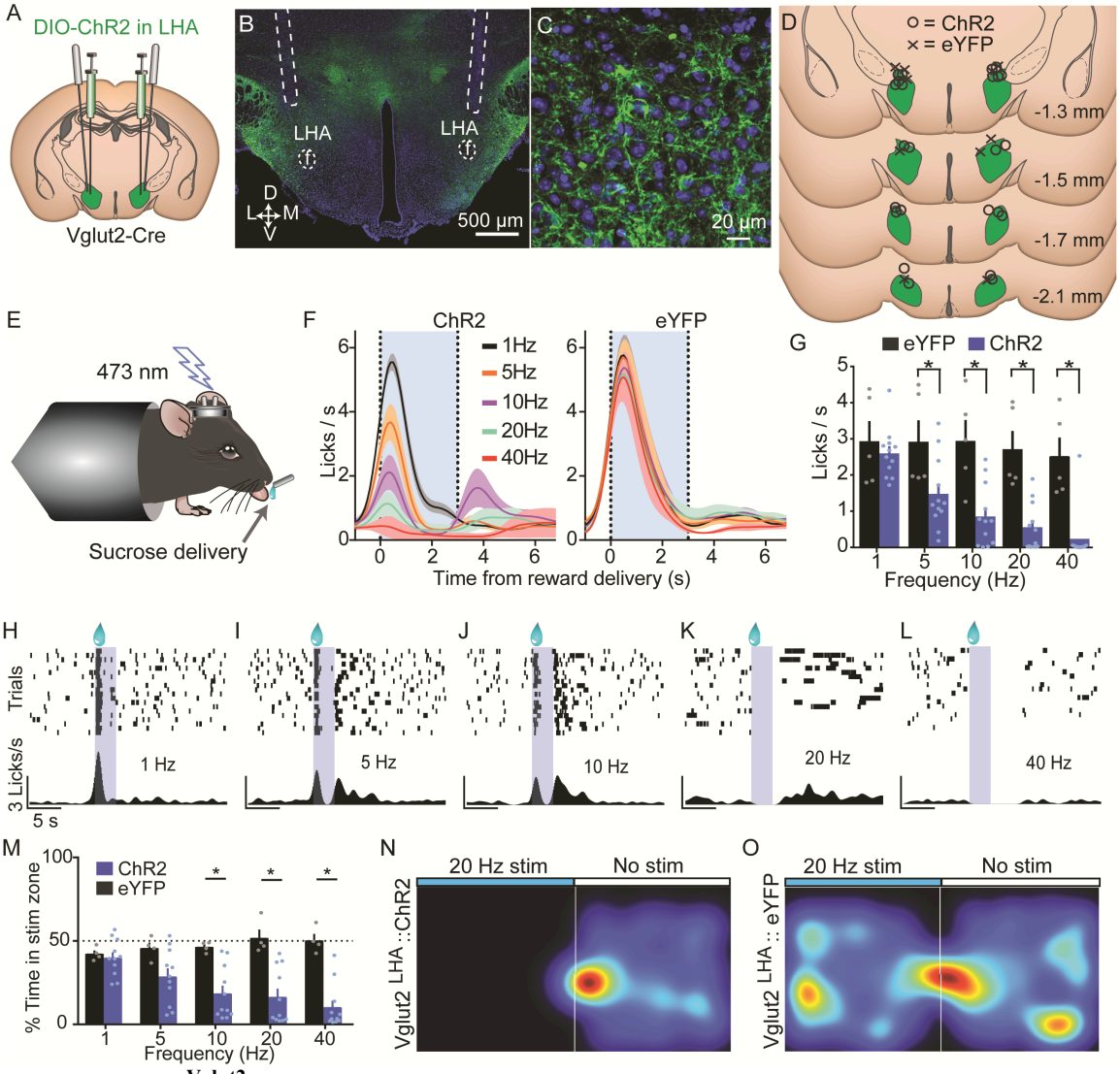


**Fig. S7. LHA$^{Vglut2}$ stimulation halts consummatory behavior and is aversive. A**. DIO-ChR2-eYFP was infused into the LHA of Vglut2-Cre mice. **B**. Optical fibers were positioned above the LHA. **C**. Example of ChR2-eFYP expression in LHA. **D.** Summary of fiber placements. **E**. Head-fixed experimental setup. 473 nm light was delivered concurrently with sucrose. **F-G**. Lick rate during stimulation was reduced in ChR2 mice (n=12) but not eYFP control mice (n=5). *$p$<0.05. **H-L**. Frequency-dependent reduction in licking for a single ChR2-expressing mouse. Licks are aligned to sucrose delivery. Stimulation occurs in the blue shaded region. **M.** Time spent on stimulation side in RTPP assay. * $p$ < 0.05. Values are mean and s.e.m. **N.** Example heatmap of ChR2 mouse position during RTPP test. **O.** Example heatmap of eYFP mouse position during RTPP test.

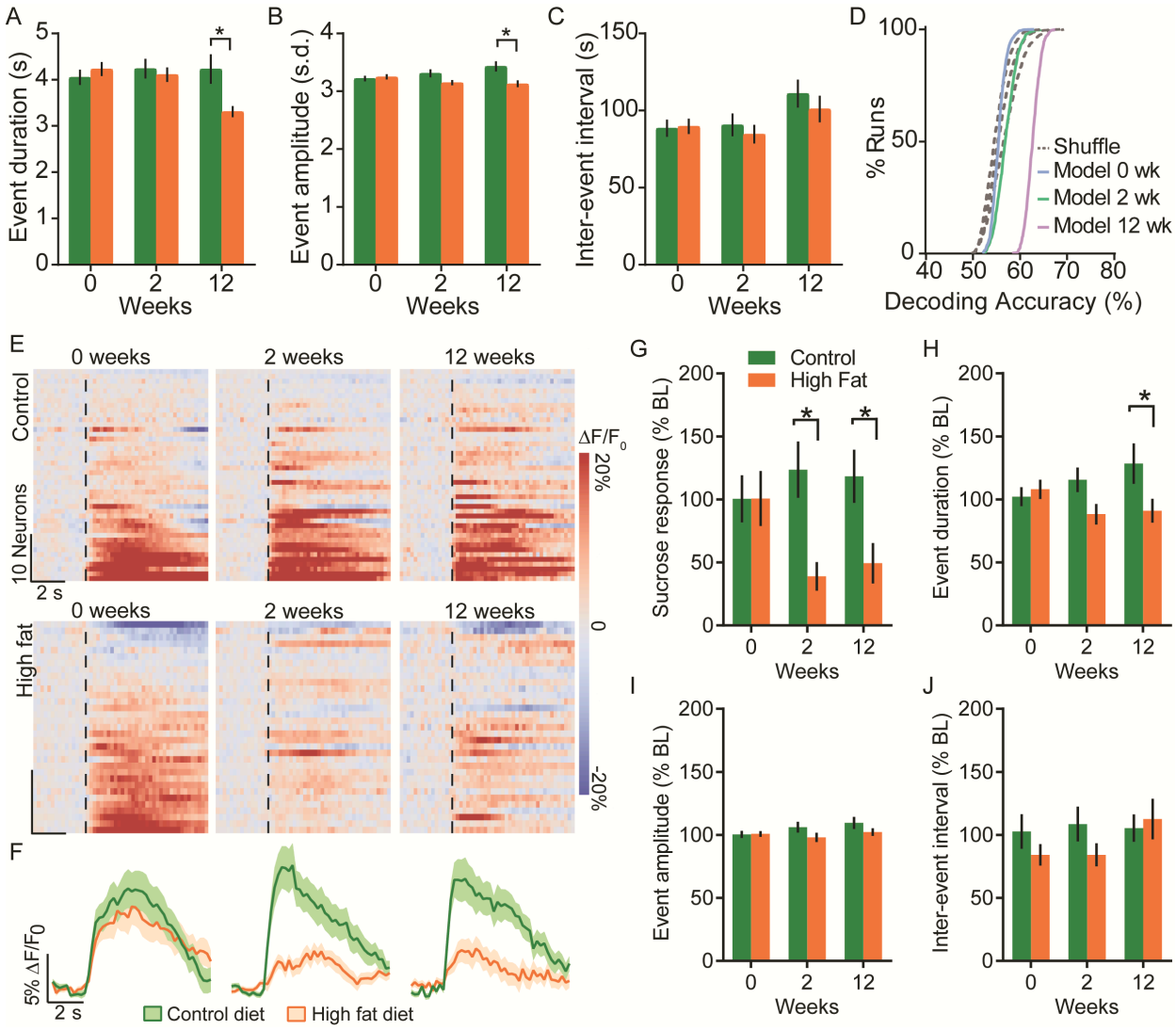


**Fig. S8. Basal activity dynamics of LHA$^{Vglut2}$ neurons during obesity and tracking LHA$^{Vglut2}$ activity dynamics during obesity. A-C.** Characterization of basal activity dynamics recorded while mice were at rest. Event duration (**A**) and event amplitude (**B**) were reduced by chronic HFD. **C.** Inter-event interval is unchanged by HFD. **D.** Decoding using event parameters was moderately successful at 12 wk ($p < 0.05$ for 12 wk vs. 0 wk and 12 wk vs. 2 wk). *$p < 0.05$. **E-G.** Sucrose evoked fluorescence from tracked cells. **E.** Heatmaps of activity from tracked neurons in control (top row) and HFD (bottom row) groups. Responses are aligned to sucrose consumption. The order of cells is maintained across the rows of heatmaps. **F.** Average sucrose response of LHA$^{Vglut2}$ neurons in control and HFD groups. **G.** Sucrose responses were reduced in the HFD

group. **H-J**. Basal activity dynamics of tracked cells. **H.** Event duration was reduced in the HFD group. Only cells with at least 1 event in each condition were included. **i.** Event amplitude was unaffected by HFD. Only cells with at least 1 event in each condition were included. **J.** Inter-event amplitude was unaffected by HFD. Only cells with at least 2 events in each condition were included. *$p < 0.05$. Values are mean and s.e.m. For **G-J**, values were normalized by the 0 week population average.

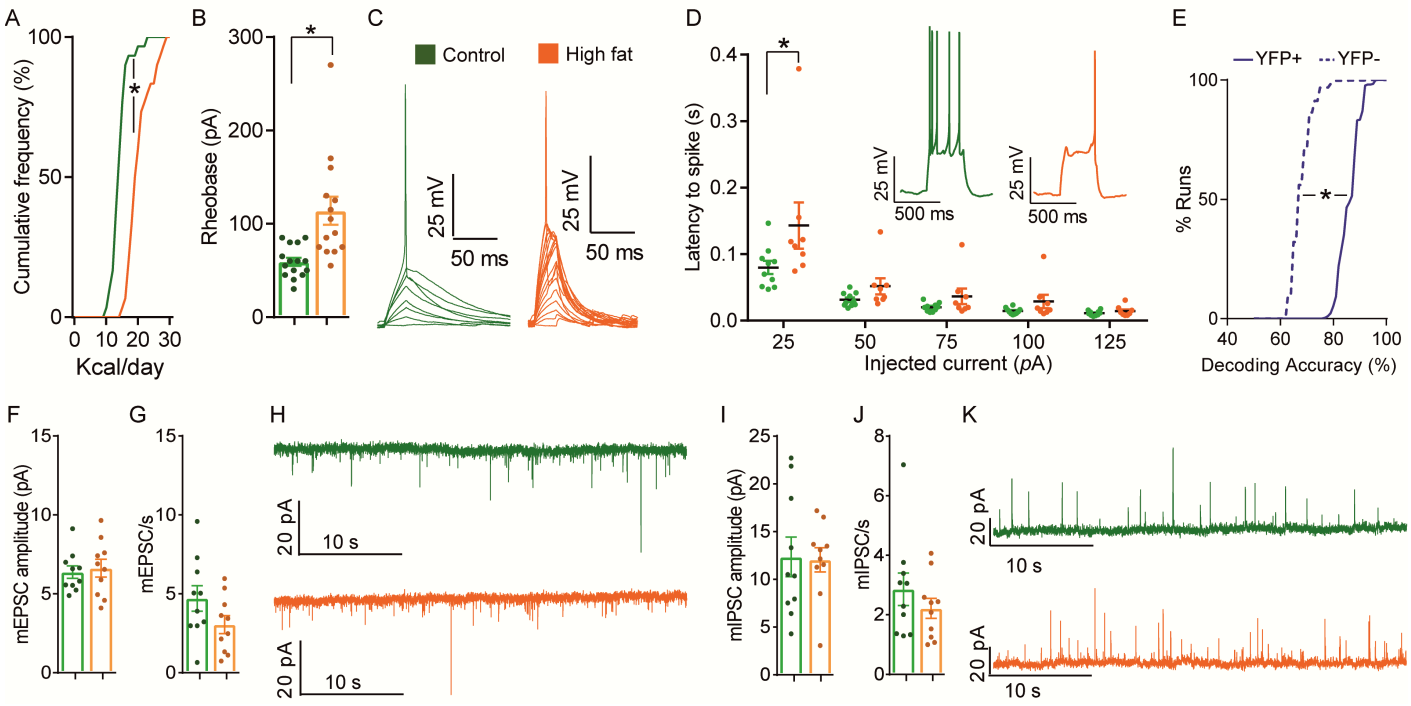


**Fig. S9. LHA$^{Vglut2}$ neurons are less excitable following chronic high fat diet. A.** Cumulative distribution of daily caloric intake (n=4/group). **B.** Rheobase was increased in LHA$^{Vglut2}$ neurons following chronic HFD exposure. One outlier was removed from the HFD group following a Grubb's test (n=15 cells from 4 control mice, n=14 cells from 4 HFD mice). **C.** Example rheobase. **D.** Latency to spike was increased in LHA$^{Vglut2}$ neurons following chronic HFD. Insets are example cells. Only cells that spiked in all conditions were included. **E.** Group assignment (control or HFD) can be more accurately decoded from the electrophysiological properties of eYFP+ cells compared with eYFP- cells. *$p$ = 0.004. **F.** mEPSC amplitude was unaffected by chronic HFD (10 cells/group from 4 mice each). **G.** mEPSC rate was unaffected by chronic HFD. **H.** Example mEPSC recording traces. **I.** mIPSC amplitude was unaffected by chronic HFD. **J.** mIPSC rate was unaffected by chronic HFD. **K.** Example mIPSC recording traces. Error bars are s.e.m.

**Table S1.**

Summary of statistical tests performed.

| Figure | | Test | N | Statistics | p | Post test | p (post) |
|---|---|---|---|---|---|---|---|
| 2 | C | Two-sample Kolmogorov-Smirnov test | GABA: 603 genes; Glut: 262 genes; Orx: 18 genes; Mch: 26 genes | Glut vs. GABA: 0.66143 | p<1.0e-15 | n/a | n/a |
| | | | | Glut vs. Orx: 0.96947 | p=3.6e-14 | n/a | n/a |
| | | | | Glut vs. Mch: 0.96947 | p<1.0e-15 | n/a | n/a |
| 3 | I | Kolmogorov-Smirnov test | 452 neurons from 13 mice | D=0.11 | p=7.92e-3 | n/a | n/a |
| | I inset | paired t test | 452 neurons from 13 mice | t(451) = 5.49 | p=6.69e-8 | n/a | n/a |
| | J | compare observations from two distributions (Runs test) | 1000 paired observations | 1000 paired observations | p=0.002 | n/a | n/a |
| 4 | B | two-way ANOVA [Group x Time] | 4-7 mice per group | Main effect of Group, F(1,31) = 8.55 | p=0.0064 | n/a | n/a |
| | | | | Main effect of Time, F(2, 31)=21.38 | p<0.0001 | n/a | n/a |
| | | | | Interaction between Group and Time, F(2, 31)=5.32 | p=0.011 | Sidak | p=0.0013 |
| | E | two-way ANOVA [Group x Time] | 0 weeks: 232 neurons from 6 control mice, 220 neurons from 7 HFD mice; 2 weeks: 188 neurons from 6 control mice, 231 neurons from 7 HFD mice; 12 weeks: 105 neurons from 4 control mice, 201 neurons from 7 HFD mice. | Main effect of Group, F(1,1171) = 45.48 | p<0.0001 | n/a | n/a |
| | | | | No main effect of Time, F(2, 1171)=1.51 | p=0.22 | n/a | n/a |
| | | | | Interaction between Group and Time, F(2, 1171)=10.99 | p<0.0001 | Sidak | p<0.0001 |

| | | | | | | | |
|---|---|---|---|---|---|---|---|
| | **F** | compare observations from two distributions (Runs test) with Benjamini-Hochberg correction (false discovery rate=0.1). | 1000 paired observations per sample | 12 vs 12 shuffled | p<0.0001 | n/a | n/a |
| | | | | 12 vs 0 | p<0.0001 | n/a | n/a |
| | | | | 12 vs 2 | p<0.0001 | n/a | n/a |
| | | | | 2 vs 2 shuffled | p=0.012 | n/a | n/a |
| | | | | 0 vs 0 shuffled | p = 0.014 | n/a | n/a |
| | | | | 0 shuffled vs 2 shuffled | p=0.474 | n/a | n/a |
| | | | | 2 vs 0 | p=0.54 | n/a | n/a |
| | | | | 0 shuffled vs 12 shuffled | p=0.578 | n/a | n/a |
| | | | | 2 shuffled vs 12 shuffled | p=0.606 | n/a | n/a |
| | **H** | linear regressions to compare slopes | Control: 44 cells from 4 mice; High fat: 33 cells from 4 mice | Control 2 wk vs control 12 wk, F(1,84)=0.48 | p=0.49 | n/a | n/a |
| | | | | High fat 2 wk vs High fat 12 wk, F(1,62)=2.70 | p=0.11 | n/a | n/a |
| | | | | High fat 2 wk vs Control 2 wk, F(1,73)=17.57 | p<0.0001 | n/a | n/a |
| | | | | High fat 12 wk vs Control 12 wk, F(1,73)=3.55 | p=0.06 | Reg. to compare intercept | p=0.0018 |
| **S1** | **A** | Repeated measures two-way ANOVA [Group x Time] | 7 mice per group | Main effect of group, F(1,12) = 88.52 | p<0.0001 | n/a | n/a |
| | | | | Main effect of Time, F(1,12)=490.7 | p<0.0001 | n/a | n/a |
| | | | | Interaction between Group and Time, F(1,12)=119.00 | p<0.0001 | Sidak | p<0.0001 |
| **S3** | **B** | t-test | 6 hemispheres from 3 mice per group | t(10)=3.78 | p=0.0036 | n/a | n/a |
| | **C** | Chi square | Control: 1514 cells<br>High fat: 1434 cells | X2(1)=95.84 | p<0.0001 | n/a | n/a |
| | **D** | two-way ANOVA [Group x Cell Type] | Control: 3887 cells<br>High fat: 3913 cells | Main effect of Group, F(1,7796) = 0.68 | p=0.4084 | n/a | n/a |
| | | | | Main effect of Cell Type, F(1,7796)=56.22 | p<0.0001 | n/a | n/a |
| | | | | Interaction between Group and Cell type, F(1,7796)=6.558 | p=0.0105 | Sidak | p=0.0333 |
| | **F** | t-test | 6 hemispheres from 3 mice per group | t(10)=2.99 | p=0.014 | n/a | n/a |

| | | | | | | | |
|---|---|---|---|---|---|---|---|
| | **G** | Chi square | Control: 1920 cells<br>High fat: 1917 cells | X2(1)=72.88 | p<0.0001 | n/a | n/a |
| | **H** | two-way ANOVA [Group x Cell Type] | Control: 3887 cells<br>High fat: 3913 cells | Main effect of group, F(1,7796) = 9.81 | p=0.0017 | n/a | n/a |
| | | | | Main effect of cell type, F(1,7796)=16.85 | p<0.0001 | n/a | n/a |
| | | | | Interaction between Group and Cell type, F(1,7796)=7.621 | p=0.0058 | Sidak | p<0.0001 |
| | **J** | t-test | 6 hemispheres from 3 mice per group | t(10)=1.88 | p=0.0897 | n/a | n/a |
| | **K** | Chi square | Control: 1552 cells<br>High fat: 1877 cells | X2(1)=28.91 | p<0.0001 | n/a | n/a |
| | **L** | two-way ANOVA [Group x Cell Type] | Control: 3887 cells<br>High fat: 3913 cells | No main effect of group, F(1,7796) = 1.62 | p=0.203 | n/a | n/a |
| | | | | Main effect of cell type, F(1,7796)=165.9 | p<0.0001 | n/a | n/a |
| | | | | No Interaction between Group and Cell type, F(1,7796)=0.6844 | p=0.4081 | n/a | n/a |
| | **N** | t-test | 6 hemispheres from 3 mice per group | t(10)=0.84 | p=0.42 | n/a | n/a |
| | **O** | Chi square | Control: 802 cells<br>High fat: 545 cells | X2(1)=2.71 | p=0.10 | n/a | n/a |
| | **P** | two-way ANOVA [Group x Cell Type] | Control: 3887 cells<br>High fat: 3913 cells | No main effect of group, F(1,7796) = 0.395 | p=0.5297 | n/a | n/a |
| | | | | Main effect of cell type, F(1,7796)=15.56 | p<0.0001 | n/a | n/a |
| | | | | No Interaction between Group and Cell type, F(1,7796)=0.201 | p=0.6541 | n/a | n/a |
| **S5** | **B** | Pearson correlation | 8 cells from 2 mice | r=0.9996 | p=0.000011 | n/a | n/a |
| | **E** | Pearson correlation | 149 trials from 13 mice | r=-0.15 | p=0.0667 | n/a | n/a |

| | | | | | | | |
|---|---|---|---|---|---|---|---|
| | **F** | Chi square | 452 cells from 13 mice | X2(2) = 15.59 | p=0.0004 | n/a | n/a |
| | **G** | Paired t-test | 331 cells from 13 mice | t(330)=2.93 | p=0.0037 | n/a | n/a |
| | **H** | Paired t-test | 331 cells from 13 mice | t(330)=2.51 | p=0.013 | n/a | n/a |
| | **I** | Paired t-test | 262 cells from 13 mice | t(261)=0.289 | p=0.77 | n/a | n/a |
| **S6** | **C** | one-way ANOVA | 7 cells from 2 mice | F(4,24) = 16.66 | p=1.16e-6 | n/a | n/a |
| | **D** | one-way ANOVA | 7 cells from 2 mice | F(4,24) = 23.66 | p=4.96e-8 | n/a | n/a |
| **S7** | **G** | repeated measures two-way ANOVA [Group x Frequency] | 5 control mice, 12 ChR2 mice | Main effect of Group, F(1,15)=15.35 | p=0.0014 | n/a | n/a |
| | | | | Main effect of Frequency, F(4,60)=14.51 | p<0.0001 | n/a | n/a |
| | | | | Interaction between Group and Frequency, F(4,60)=8.18 | p<0.0001 | Sidak | p<0.05 |
| | **M** | repeated measures two-way ANOVA [Group x Frequency] | 4 control mice, 11 ChR2 mice | Main effect of Group, F(1,13)=15.49 | p=0.0017 | n/a | n/a |
| | | | | Main effect of Frequency, F(4,52)=2.62 | p=0.045 | n/a | n/a |
| | | | | Interaction between Group and Frequency, F(4,52)=8.36 | p<0.0001 | Sidak | p<0.05 |
| **S8** | **A** | two-way ANOVA [Group x Time] | 0 weeks: 204 neurons from 6 control mice, 176 neurons from 7 HFD mice; 2 weeks: 137 neurons from 6 control mice, 163 neurons from 7 HFD mice; 12 weeks: 79 neurons from 4 control mice, 131 neurons from 7 HFD mice. | No main effect of group, F(1,884) = 3.61 | p=0.058 | n/a | n/a |
| | | | | No main effect of Time, F(2, 884)=2.42 | p=0.09 | n/a | n/a |
| | | | | Interaction between Group and Time, F(2, 884)=4.17 | p=0.0158 | Sidak | p=0.0092 |

| | | | | | | | |
|---|---|---|---|---|---|---|---|
| | **B** | two-way ANOVA [Group x Time] | 0 weeks: 204 neurons from 6 control mice, 176 neurons from 7 HFD mice; 2 weeks: 137 neurons from 6 control mice, 163 neurons from 7 HFD mice; 12 weeks: 79 neurons from 4 control mice, 131 neurons from 7 HFD mice. | Main effect of Group, F(1,884) = 9.13 | p=0.0026 | n/a | n/a |
| | | | | No main effect of Time, F(2, 884)=0.38 | p=0.69 | n/a | n/a |
| | | | | Interaction between Group and Time, F(2, 884)=4.18 | p=0.0157 | Sidak | p=0.0057 |
| | **C** | two-way ANOVA [Group x Time] | 0 weeks: 175 neurons from 6 control mice, 152 neurons from 7 HFD mice; 2 weeks: 116 neurons from 6 control mice, 124 neurons from 7 HFD mice; 12 weeks: 64 neurons from 4 control mice, 99 neurons from 7 HFD mice. | No main effect of Group, F(1,724) = 0.749 | p=0.387 | n/a | n/a |
| | | | | Main effect of Time, F(2, 724)=3.56 | p=0.029 | n/a | n/a |
| | | | | No interaction between Group and Time, F(2, 724)=0.369 | p=0.69 | n/a | n/a |
| | **D** | compare observations from two distributions (Runs test) with Benjamini-Hochberg correction (false discovery rate=0.1). | 1000 paired observations per sample | 12 vs 0 | p=0.002 | n/a | n/a |
| | | | | 12 vs 2 | p=0.017 | n/a | n/a |
| | | | | 12 vs 12 shuffled | p=0.052 | n/a | n/a |
| | | | | 2 vs 0 | p=0.285 | n/a | n/a |
| | | | | 2 vs 2 shuffled | p = 0.316 | n/a | n/a |
| | | | | 0 vs 0 shuffled | p=0.37 | n/a | n/a |
| | | | | 0 shuffled vs 2 shuffled | p=0.57 | n/a | n/a |
| | | | | 2 shuffled vs 12 shuffled | p=0.594 | n/a | n/a |
| | | | | 0 shuffled vs 12 shuffled | p=0.665 | n/a | n/a |

| | | | | | | | |
|---|---|---|---|---|---|---|---|
| | **G** | Repeated measures two-way ANOVA [Group x Time] | Control: 44 cells from 4 mice; High fat: 33 cells from 4 mice | Main effect of group, F(1,75) = 4.27 | p=0.0422 | n/a | n/a |
| | | | | No main effect of Time, F(2, 150)=1.67 | p=0.19 | n/a | n/a |
| | | | | Interaction between Group and Time, F(2, 150)=7.75 | p=0.0006 | Sidak | p=0.0086<br>p=0.0433 |
| | **H** | Repeated measures two-way ANOVA [Group x Time] | Control: 30 cells from 4 mice; High fat: 26 cells from 4 mice | No main effect of group, F(1,54) = 3.54 | p=0.0654 | n/a | n/a |
| | | | | No main effect of Time, F(2, 108)=0.38 | p=0.68 | n/a | n/a |
| | | | | Interaction between Group and Time, F(2, 108)=3.11 | p=0.048 | Sidak | p=0.0365 |
| | **I** | Repeated measures two-way ANOVA [Group x Time] | Control: 30 cells from 4 mice; High fat: 26 cells from 4 mice | No main effect of group, F(1,54) = 2.21 | p=0.14 | n/a | n/a |
| | | | | No main effect of Time, F(2, 108)=1.26 | p=0.29 | n/a | n/a |
| | | | | No Interaction between Group and Time, F(2, 108)=0.95 | p=0.39 | n/a | n/a |
| | **J** | Repeated measures two-way ANOVA [Group x Time] | Control: 26 cells from 4 mice; High fat: 19 cells from 4 mice | No main effect of group, F(1,43) = 1.02 | p=0.32 | n/a | n/a |
| | | | | No main effect of Time, F(2,86)=0.97 | p=0.38 | n/a | n/a |
| | | | | No Interaction between Group and Time, F(2,86)=1.00 | p=0.37 | n/a | n/a |
| **S9** | **A** | Kolmogorov-Smirnov test | 4 mice per group | D=0.833 | p=1.79e-9 | n/a | n/a |
| | **B** | Grubbs test to identify outliers | 15 cells per group | Grubb (alpha = 0.05) = 1 outlier | p<0.05 | n/a | n/a |
| | **B** | t-test | Control: 15 cells High fat: 14 cells | t(27)=3.56 | p=0.00139 | n/a | n/a |
| | **D** | Repeated measures two-way ANOVA [Group x Current] | Control: 10 cells High fat: 8 cells | No main effect of group, F(1,16) =3.48 | p=0.08 | n/a | n/a |
| | | | | Main effect of Current, F(4, 64)=40.41 | p<0.0001 | n/a | n/a |
| | | | | Interaction between Group and Frequency, F(4, 64)=3.43 | p=0.0133 | Sidak | p=0.0016 |

| | | | | | | | |
|---|---|---|---|---|---|---|---|
| | **E** | compare observations from two distributions (Runs test) | 1000 paired observations | 1000 paired observations | p=0.004 | n/a | n/a |
| | **F** | t-test | 10 cells per group | t(18)=0.355 | p=0.73 | n/a | n/a |
| | **G** | t-test | 10 cells per group | t(18)=1.68 | p=0.11 | n/a | n/a |
| | **I** | t-test | 10 cells per group | t(18)=0.12 | p=0.90 | n/a | n/a |
| | **J** | t-test | 10 cells per group | t(18)=1.01 | p=0.33 | n/a | n/a |

**Supplementary Data S1 (separate file)**

Differential gene expression values across clusters. Includes p-values from the likelihood ratio test for single-cell data for each gene by cluster, asinh fold-changes for each gene by cluster, and percent of cells expressing each gene per cluster.

**Supplementary Data S2 (separate file)**

Functional annotation results for glutamatergic, GABAergic, and oligodendrocyte clusters and likelihood ratio test p-values for late vs early pseudotime LHA$^{Vglut2}$ HFD cells.

**References**


1. M. M. Finucane *et al.*, National, regional, and global trends in body-mass index since 1980: systematic analysis of health examination surveys and epidemiological studies with 960 country-years and 9.1 million participants. *Lancet* **377**, 557-567 (2011).
2. P. G. Kopelman, Obesity as a medical problem. *Nature* **404**, 635-643 (2000).
3. B. G. Hoebel, P. Teitelbaum, Hypothalamic control of feeding and self-stimulation. *Science* **135**, 375-377 (1962).
4. M. A. Rossi, G. D. Stuber, Overlapping Brain Circuits for Homeostatic and Hedonic Feeding. *Cell Metab*, (2017).
5. R. A. Wise, Hypothalamic motivational systems: fixed or plastic neural circuits? *Science* **162**, 377-379 (1968).
6. D. L. Margules, J. Olds, Identical "feeding" and "rewarding" systems in the lateral hypothalamus of rats. *Science* **135**, 374-375 (1962).
7. B. K. Anand, S. Dua, K. Shoenberg, Hypothalamic control of food intake in cats and monkeys. *J Physiol* **127**, 143-152 (1955).
8. J. H. Jennings, G. Rizzi, A. M. Stamatakis, R. L. Ung, G. D. Stuber, The inhibitory circuit architecture of the lateral hypothalamus orchestrates feeding. *Science* **341**, 1517-1521 (2013).
9. J. H. Jennings *et al.*, Visualizing hypothalamic network dynamics for appetitive and consummatory behaviors. *Cell* **160**, 516-527 (2015).
10. A. M. Stamatakis *et al.*, Lateral Hypothalamic Area Glutamatergic Neurons and Their Projections to the Lateral Habenula Regulate Feeding and Reward. *J Neurosci* **36**, 302-311 (2016).
11. E. H. Nieh *et al.*, Decoding neural circuits that control compulsive sucrose seeking. *Cell* **160**, 528-541 (2015).
12. E. Z. Macosko *et al.*, Highly Parallel Genome-wide Expression Profiling of Individual Cells Using Nanoliter Droplets. *Cell* **161**, 1202-1214 (2015).
13. R. Satija, J. A. Farrell, D. Gennert, A. F. Schier, A. Regev, Spatial reconstruction of single-cell gene expression data. *Nat Biotechnol* **33**, 495-502 (2015).
14. F. E. Henry, K. Sugino, A. Tozer, T. Branco, S. M. Sternson, Cell type-specific transcriptomics of hypothalamic energy-sensing neuron responses to weight-loss. *Elife* **4**, (2015).
15. R. Chen, X. Wu, L. Jiang, Y. Zhang, Single-Cell RNA-Seq Reveals Hypothalamic Cell Diversity. *Cell Rep* **18**, 3227-3241 (2017).
16. C. Trapnell *et al.*, The dynamics and regulators of cell fate decisions are revealed by pseudotemporal ordering of single cells. *Nat Biotechnol* **32**, 381-386 (2014).
17. M. V. Kuleshov *et al.*, Enrichr: a comprehensive gene set enrichment analysis web server 2016 update. *Nucleic Acids Res* **44**, W90-97 (2016).
18. J. A. McHenry *et al.*, Hormonal gain control of a medial preoptic area social reward circuit. *Nat Neurosci* **20**, 449-458 (2017).
19. J. M. Otis *et al.*, Prefrontal cortex output circuits guide reward seeking through divergent cue encoding. *Nature* **543**, 103-107 (2017).
20. E. H. Nieh *et al.*, Inhibitory Input from the Lateral Hypothalamus to the Ventral Tegmental Area Disinhibits Dopamine Neurons and Promotes Behavioral Activation. *Neuron* **90**, 1286-1298 (2016).

21. I. Lazaridis *et al.*, A hypothalamus-habenula circuit controls aversion. *Mol Psychiatry*, (2019).
22. M. Trusel *et al.*, Punishment-Predictive Cues Guide Avoidance through Potentiation of Hypothalamus-to-Habenula Synapses. *Neuron*, (2019).
23. L. E. Mickelsen *et al.*, Single-cell transcriptomic analysis of the lateral hypothalamic area reveals molecularly distinct populations of inhibitory and excitatory neurons. *Nat Neurosci* **22**, 642-656 (2019).
24. L. Vong *et al.*, Leptin action on GABAergic neurons prevents obesity and reduces inhibitory tone to POMC neurons. *Neuron* **71**, 142-154 (2011).
25. D. R. Sparta *et al.*, Construction of implantable optical fibers for long-term optogenetic manipulation of neural circuits. *Nat Protoc* **7**, 12-23 (2011).
26. T. W. Chen *et al.*, Ultrasensitive fluorescent proteins for imaging neuronal activity. *Nature* **499**, 295-300 (2013).
27. S. L. Resendez *et al.*, Visualization of cortical, subcortical and deep brain neural circuit dynamics during naturalistic mammalian behavior with head-mounted microscopes and chronically implanted lenses. *Nat Protoc* **11**, 566-597 (2016).
28. J. T. Ting, T. L. Daigle, Q. Chen, G. Feng, Acute brain slice methods for adult and aging animals: application of targeted patch clamp analysis and optogenetics. *Methods Mol Biol* **1183**, 221-242 (2014).
29. W. E. Johnson, C. Li, A. Rabinovic, Adjusting batch effects in microarray expression data using empirical Bayes methods. *Biostatistics* **8**, 118-127 (2007).
30. J. T. Leek, W. E. Johnson, H. S. Parker, A. E. Jaffe, J. D. Storey, The sva package for removing batch effects and other unwanted variation in high-throughput experiments. *Bioinformatics* **28**, 882-883 (2012).
31. P. Brennecke *et al.*, Accounting for technical noise in single-cell RNA-seq experiments. *Nat Methods* **10**, 1093-1095 (2013).
32. T. S. Andrews, M. Hemberg, M3Drop: Dropout-based feature selection for scRNASeq. *Bioinformatics*, (2018).
33. A. McDavid *et al.*, Data exploration, quality control and testing in single-cell qPCR-based gene expression experiments. *Bioinformatics* **29**, 461-467 (2013).
34. M. M. Hoffman *et al.*, Unsupervised pattern discovery in human chromatin structure through genomic segmentation. *Nat Methods* **9**, 473-476 (2012).
35. C. A. de Leeuw, J. M. Mooij, T. Heskes, D. Posthuma, MAGMA: generalized gene-set analysis of GWAS data. *PLoS Comput Biol* **11**, e1004219 (2015).
36. N. G. Skene *et al.*, Genetic identification of brain cell types underlying schizophrenia. *Nat Genet* **50**, 825-833 (2018).
37. C. J. Willer, Y. Li, G. R. Abecasis, METAL: fast and efficient meta-analysis of genomewide association scans. *Bioinformatics* **26**, 2190-2191 (2010).
38. B. K. Bulik-Sullivan *et al.*, LD Score regression distinguishes confounding from polygenicity in genome-wide association studies. *Nat Genet* **47**, 291-295 (2015).
39. K. Watanabe, E. Taskesen, A. van Bochoven, D. Posthuma, Functional mapping and annotation of genetic associations with FUMA. *Nat Commun* **8**, 1826 (2017).
40. S. McCarthy *et al.*, A reference panel of 64,976 haplotypes for genotype imputation. *Nat Genet* **48**, 1279-1283 (2016).
41. C. Bycroft *et al.*, Genome-wide genetic data on ~500,000 UK Biobank participants. *bioRxiv*, (2017).